ADVANCED MATERIALS

Supporting Information

for *Adv. Mater.*, DOI: 10.1002/adma.201500533

Sensing Solvents with Ultrasensitive Porous Poly(ionic liquid) Actuators

*Qiang Zhao, Jan Heyda, Joachim Dzubiella, Karoline Täuber, John W. C. Dunlop, and Jiayin Yuan**

Supporting Information

Sensing solvents with ultra-sensitive porous poly(ionic liquid) actuators

Qiang Zhao,[a] Jan Heyda,[b,e] Joachim Dzubiella,[b,c] Karoline Täuber,[a] John W.C. Dunlop[d] and Jiayin Yuan*[a]

1. Chemicals, polymers and characterizations

Poly(acrylic acid) (PAA, solid powder, MW=2000 Da), lithium bis(trifluoro methanesulfonyl)imide ($LiTf_2N$, 99.95%), aqueous ammonia (28 w%) were purchased from Sigma-Aldrich and used without further purification. All organic solvents were of analytic grade.

FT-IR spectra were performed on a BioRad 6000 FT-IR spectrometer; samples were measured in solid state using a Single Reflection Diamond ATR. Scanning electron microscopy (SEM) was performed on a GEMINI LEO 1550 microscope at 3 kV. Samples were coated with a thin layer of gold before examination. Element (sulfur) analysis of the membrane cross-section was measured by means of EDX (Oxford instruments) via scanning electron microscopy (DSM 940A, Carl Zeiss AG). Poly(3-cyanomethyl-1-vinylimidazolium bis(trifluoromethanesulfonyl)imide), $PCMVImTf_2N$, was synthesized via the method in our previous study (*Chem. Mater. 2010, 22, 5003–5012*), and characterized by the proton nuclear magnetic resonance (^{1}H-NMR, **Figure S1**). Its apparent molecular weight and PDI were 1.15 × 10^5 g/mol and 2.95, respectively.

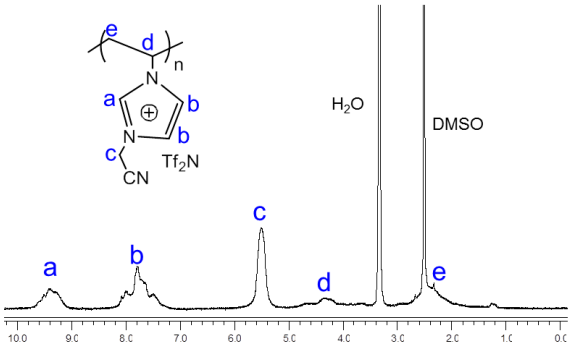

Figure S1. Chemical structures and ^{1}H-NMR spectra of poly(3-cyanomethyl-1-vinylimidazolium bis(trifluoromethanesulfonyl)imide), $PCMVImTf_2N$.

2. Preparation and characterization of PCMVImTf$_2$N-PAA membranes

The actuator membranes were prepared in a method reported previously (**Figure S2**). Typically, PCMVImTf$_2$N (1.0 g) and PAA (0.18 g) were dissolved in 10 mL of dimethylformamide (DMF) solvent, forming a homogeneous solution. Then the solution was cast onto a clean glass plate, dried at 80 ^{o}C for 1h, and soaked in aqueous ammonia (0.2 wt%, 20 ^{o}C, 2 h). After the soaking step, a free-standing membrane was easily peeled off from the glass substrate (denoted as PCMVImTf$_2$N-PAA). The as-prepared membrane features a nanoporous structure (**Figure S3**). As a result of the pore formation, not surprisingly there is an increase (35 ± 5 %) in membrane thickness after it was treated by aqueous ammonia.

Moreover, when soaking in aqueous ammonia, the ammonia molecules will diffuse into the membrane, and deprotonate the COOH groups on PAA into COO^{-}NH$_4^{+}$, thus triggering its electrostatic complexation with cationic PCMVImTf$_2$N polymers. As such, the membrane was found to be stable (not to be dissolved) in almost all common organic solvents, indicative of the effective cross-linking via electrostatic interaction.

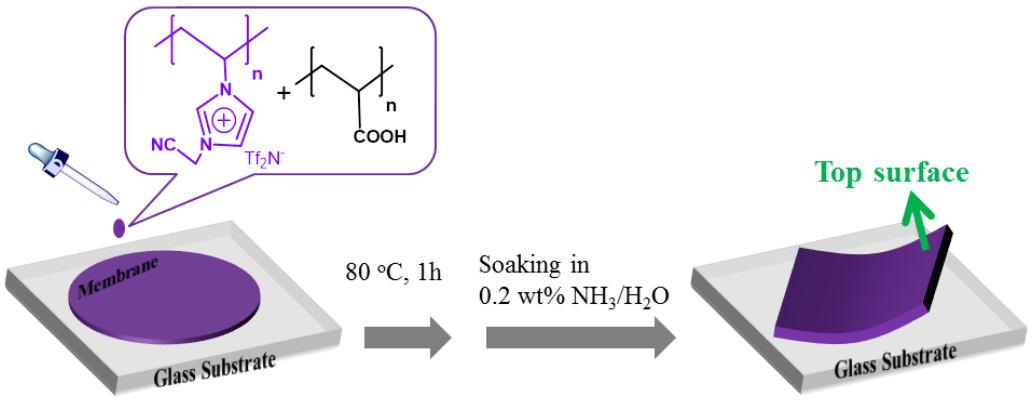

Figure S2. Schematic preparation of a PCMVImTf$_2$N-PAA membrane actuator. Note: the membrane surfaces facing the aqueous ammonia and glass plate during the soaking step are denoted as TOP and BOTTOM surfaces, respectively.

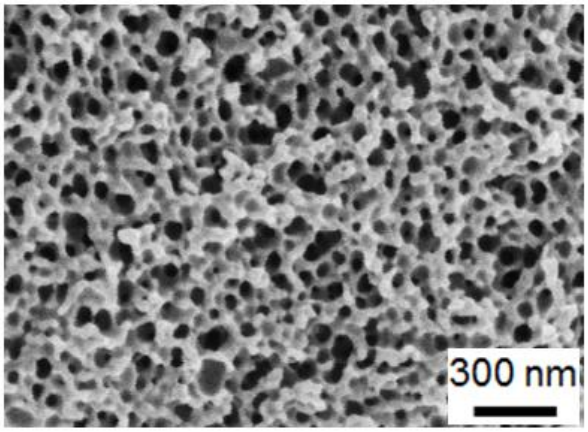

Figure S3. Cross-sectional SEM morphology of a PCMVImTf_2N-PAA membrane.

The degree of electrostatic complexion (DEC) of the membrane is defined as the ratio of the imidazolium units that ***undergo electrostatic complexation with*** $COO^-NH_4^+$ ***groups*** to the overall number of imidazolium units (**Figure S4**).

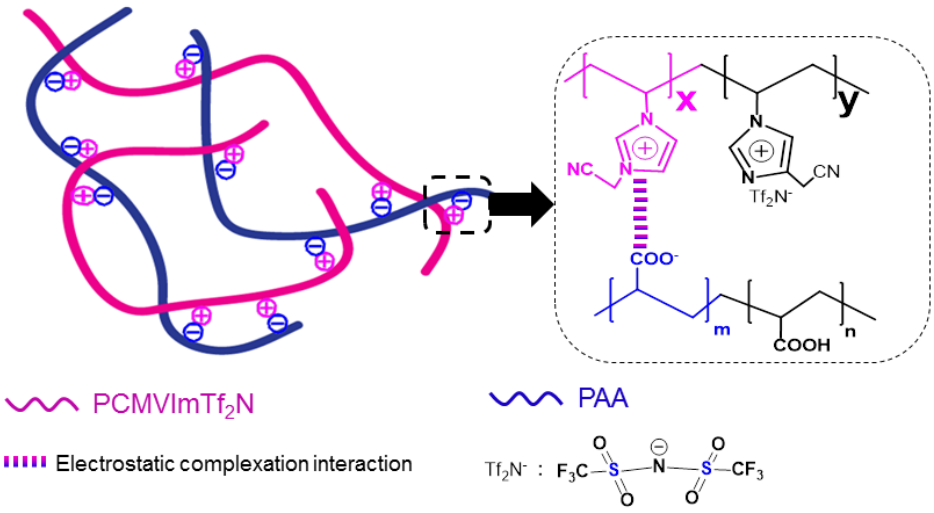

$$DEC = X/(X+Y) \quad (1)$$

$$DEC = (280-486S)/(280-280S) \quad (S: \text{sulfur weight content}) \quad (2)$$

Figure S4. (top) A scheme for defining the degree of electrostatic complexation (DEC) of the membrane; (bottom) equations for defining (eq. 1) and calculating (eq. 2) DEC.

Thus, DEC is expressed in equation (1); whereas, ***X*** denotes the imidazolium units that undergo electrostatic complexation with $COO^-NH_4^+$ groups on PAA; ***Y*** denotes the

imidazolium units that are **NOT** involved in the electrostatic complexation. Note that the electrostatic complexation is accompanied by the release of [Tf_2N^-] anions. Thus the value of DEC can be calculated from the content of sulfur element because sulfur exists only in [Tf_2N^-] counter anion. As such DEC values at different locations of the membrane are experimentally determined by equation (2), in which ***S*** is the sulfur content at different locations of the membrane cross-section measured by EDX. **Figure S5** shows the sulfur content along the membrane cross-section; indicating that the DEC decreases with the top-down depth along the cross-section. This DEC gradient is consistent with the membrane formation mechanism. Ammonia diffuses into the membrane from the top surface (membrane-liquid interface) and deprotonates the COOH groups on PAA into carboxylate groups ($COO^-NH_4^+$), thus the DEC is higher at the places closer to the top surfaces.

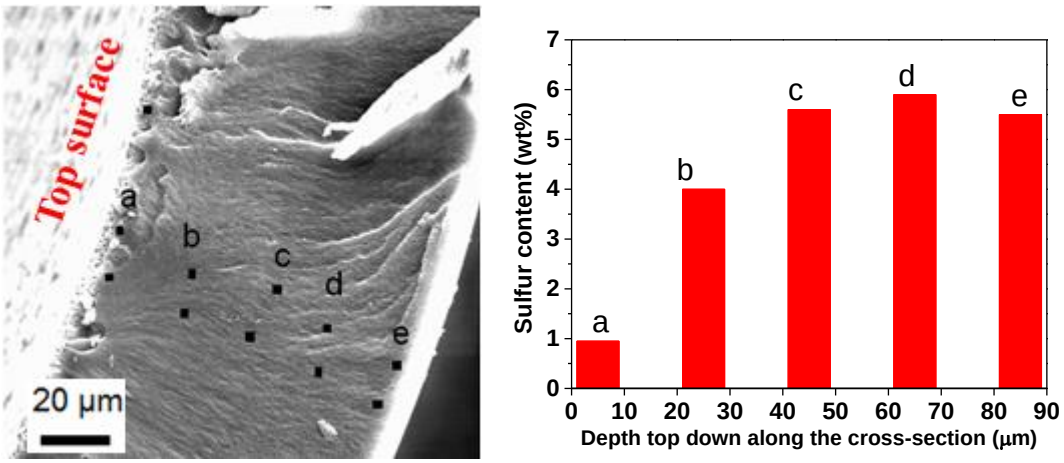

Figure S5. Sulfur content at different locations along the cross-section of the membrane actuator from the top to the bottom. On the left is the SEM picture of the membrane cross-section and the positions (a - e) taken for element analysis. Please note: here the membrane sample for measuring the cross-sectional compositions is ca. 90 μm thick. This membrane is thicker than membranes for actuation experiments (ca. 30μm), so that more positions along the cross-section can be tested.

3. Actuation of PCMVImTf2N-PAA membrane actuators.

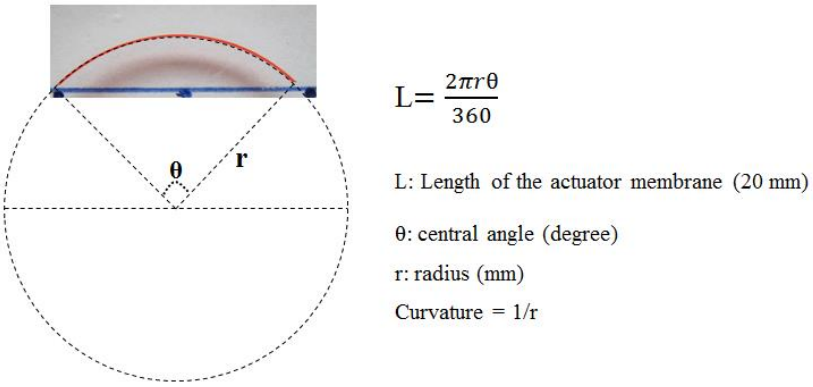

Figure S6. Measuring the central angle (θ, degree) of PCMVImTf$_2$N-PAA membrane (1 mm × 20 mm × 30 μm) placed in 0.25 mol% acetone-water mixture at 20 ^{o}C. Note: curvature was calculated through equations on the right side. Curvatures of all membrane arches in Figure 1 were obtained in the same way.

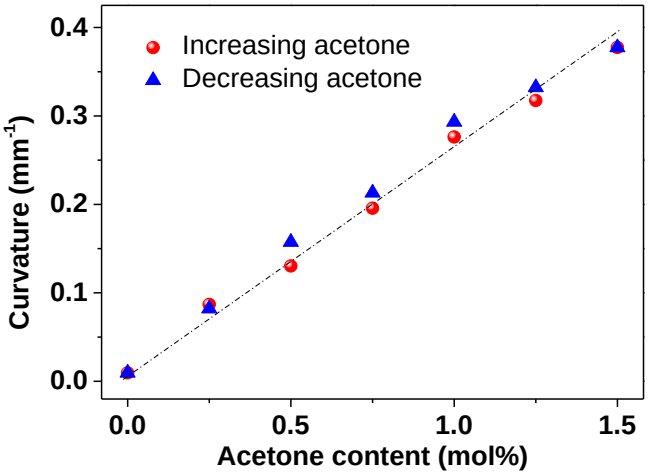

Figure S7. Curvature of a PCMVImTf$_2$N-PAA membrane actuator versus acetone content after 20 times cycling, for increasing (red) and decreasing (blue) acetone content from 0 to 1.5 mol%.

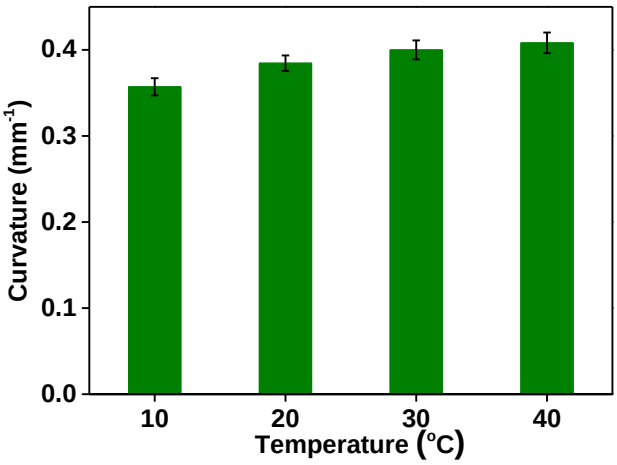

Figure S8. Variation of curvature of a PCMVImTf_2N-PAA membrane (1 mm × 20 mm × 30 μm) in 1.5 mol% acetone-water mixture at different temperatures.

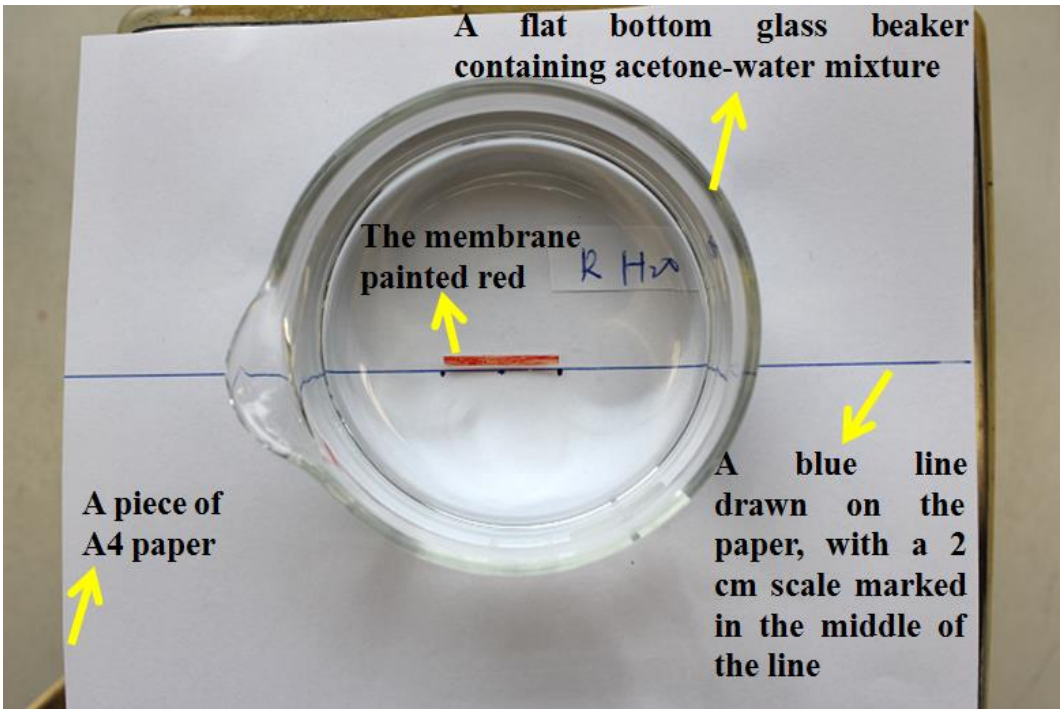

Figure S9. A photograph (top view) of the experimental setup for Figure 1a. Please note: the glass beaker was sealed during the experiment.

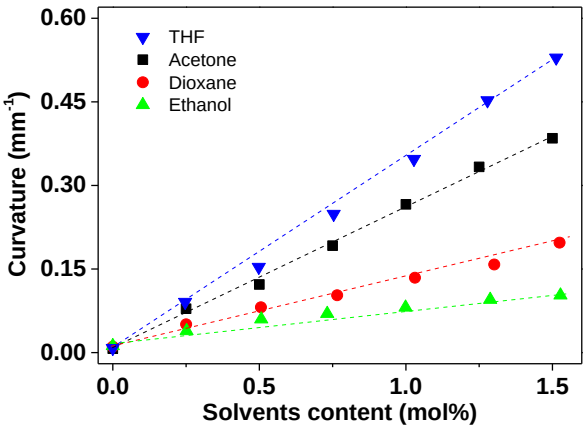

Figure S10. Effect of solvents (THF, acetone, dioxane, ethanol) content on curvature of PCMVImTf2N-PAA membrane actuator (1 mm × 20 mm × 30 μm), respectively.

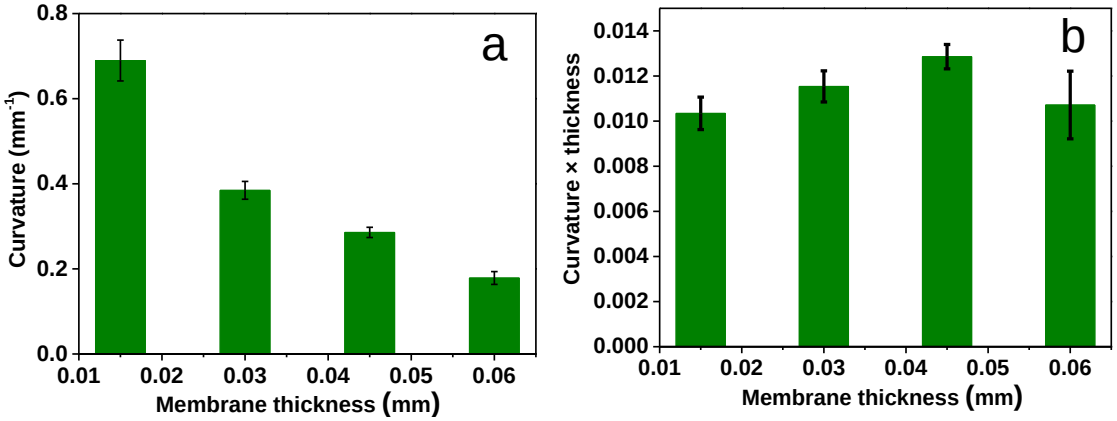

Figure S11. Effect of thickness of the PCMVImTf2N-PAA membrane actuator (1 mm × 20 mm) on its bending curvature (a) and normalized curvature (b) in 1.5 mol% acetone-water mixture at 20 ^{o}C.

Table S1. Comparison of the sensitivity of PCMVImTf_2N-PAA actuator with relevant literature data published recently.

Materials	Organic solvents	Membrane thickness (mm)	Apparent Sensitivity [a]	Normalized Sensitivity [b]	Ref
Porous PCMVImTf_2N-PAA films	Acetone	0.03	0.256	7.68×10^{-3}	This work
Bilayer phenol-formaldehyde	Acetone	0.045	0.0071	3.19×10^{-4}	[S1]

films.					
PTMSDPA/BOPP bilayer films [c]	Acetone	0.0245	-0.017	$-.4.17 \times 10^{-4}$	[S2]
Poly(nOBA/C6M)$^{-}$ K^{+} films	Acetone	0.018	0.0042	7.56×10^{-4}	[S3]

a: Apparent sensitivity is defined as the change of curvature achieved by adding 1 mol% organic solvents, i.e., the amount of curvature change (△c) divided by the amount of added solvent (S, mol%): △c/S. Please note: positive value of sensitivity means the membrane is straight in water and bends upon adding organic solvents; negative value of sensitivity means the membrane is curved in water and unbends upon adding organic solvents.

b: Normalized sensitivity equals apparent sensitivity multiplied by thickness.

c: PTMSDPA: poly[1-phenyl-2-(p -trimethylsilyl)phenylacetylene]; BOPP: biaxially oriented polypropylene

Figure S12. An optical photograph of a piece of PCMVImTf_2N-PAA membrane (dense structure, without electrostatic complexation) placed in 1.5 mol% acetone-water mixture at 20 ^{o}C. Note: the membrane in Figure S12 was not painted with red color and shows its original yellowish color.

4. Molecular dynamics (MD) computer simulations of PIL-ion pair in water-butanol mixtures.

Consistently with our recent publication,[S4] a single pair of the ionic liquid (IL) cation [3-cyanomethyl-1-vinylimidazolium] (CMVIm)] and anion bis(trifluoromethanesulfonyl)imide

(bistriflate anion, Tf_2N) in water mixed with butanol was investigated in terms of all-atom MD simulation. The preferential interaction between the PIL-ion pair and three butanol isomers were individually calculated and compared, namely: 1-butanol (IUPAC: but-1-ol), 2-butanol (but-2-ol), terc-butanol (2-methyl-prop-2-ol). The simulations were performed with the Gromacs 4.5.3 simulation package[S5] using the all-atom OPLS (nonpolarizable) force field.

The force field of the Tf_2N anion and imidazolium-based IL was described as put forward recently.[S6] The *1*- and *terc*-butanol force fields were taken from a recently developed solvent database,[S7] which uses the OPLSAA atom types. The force field for 2-butanol was not available, therefore it was built from force-field of 1-butanol, since both alcohols possesses the same atom types. The partial charges were distributed on all butanol isomers in the same way: H(C)=0.06e, C(H)=-n*0.06e (n is the number of covalently bound hydrogens to carbon atom), O(H)=-0.683e, H(O)=0.418e, and partial charge on C(OH) was determined so that the whole alcohol molecule is electroneutral.

The simulations were performed in the constant temperature and constant pressure Gibbs ensemble. Temperature and pressure at ambient conditions (300 K and 101 kPa) were controlled by a weak velocity rescale coupling scheme,[S8] and the Parinello-Rahmann barostat,[S9] respectively. Electrostatic interactions were properly calculated by the particle mesh Ewald summation with standard cut-off and grid parameters.[S6] The integration time step in the simulations was 2 fs and we gathered statistics every 1 ps. We first performed a 20 ns equilibration phase of all systems, which was followed by an at least 80 ns of production phase, in order to obtain properly converged radial distribution functions for ions and solute. To avoid finite size effects in solution structure, we studied relatively large systems with an equilibrium length of approx. 4.5 nm of the cubic and periodically repeated box. Here, a

single cation-anion pair was immersed in 2760 SPC/E water molecules,[S10] and 30 or 60 butanol molecules, giving rise to a butanol molar density of 0.6M, and 1.2M respectively.

From the solution structure, the solvation properties, in particular the excess adsorption of butanol over water (i.e. replacement of solvent by cosolvent), can be obtained as detailed in the following.

3.1. Analysis of simulation data

From the simulations we calculated the average structure of water (W) and butanol (S) around the PIL-cation/anion (+ and -) in terms of the radial pair distribution functions between the ions (+,-) and the solvents (W,S) $g_{-W}(r), g_{+W}(r), g_{-S}(r), g_{+S}(r)$. The results gathered for two concentrations were compared and evaluated.

The water and cosolvent adsorption (with respect to an ideal gas), also known as excess coordination number, N_{ij}^{ex},[S11] is then defined by volume integration over the PIL-cation/anion-water ($g_{iW}(r)-1$) and PIL-cation/anion -cosolvent ($g_{iS}(r)-1$) structure, multiplied by the density ρ_W *and* ρ_S *, respectively.*

$$N_{iS}^{ex} = 4\pi\rho_S \int_0^\infty (g_{iS}(r) - 1)r^2 \mathrm{d}r \qquad (S-MD1)$$

$$N_{iW}^{ex} = 4\pi\rho_W \int_0^\infty (g_{iW}(r) - 1)r^2 \mathrm{d}r$$

The cosolvent adsorption for the PILion-pair, N_{iS}^{ex}, is then obtained as the sum of contribution from cation and anion respectively:

$$N_S^{ex} = N_{+S}^{ex} + N_{-S}^{ex} \qquad (S-MD2),$$

and the water adsorption is obtained analogously.

Another important thermodynamic quantity in water:cosolvent mixtures is the excess adsorption of cosolvent with respect to the water, also known as preferential binding

coefficient Γ_{ij}. This is defined by the volume integration of the solute-solvent and solute-cosolvent structure difference ($g_{iS}(r)$- $g_{iW}(r)$) and multiplied by the cosolvent density ρ_S

$$\Gamma_{iS} = 4\pi\rho_S \int_0^\infty \left(g_{iS}(r) - g_{iW}(r)\right) r^2 \mathrm{d}r \qquad (S-MD3)$$

The solvent excess adsorption for the PILion-pair, Γ_S , is again obtained as the sum

$$\Gamma_S = \Gamma_{+S} + \Gamma_{-S} \qquad (S-MD4).$$

All these thermodynamic parameters are summarized in the **Table S1** and plotted in **Figure S16** with respect to butanol concentration.

3.2. Results

Applying MD simulations, we have quantified the structure around the PIL cation and anion in terms of radial distribution functions at two butanol concentrations (0.6 M and 1.2 M). Results of the structure are presented in **Figure S13** and **Figure S14**.

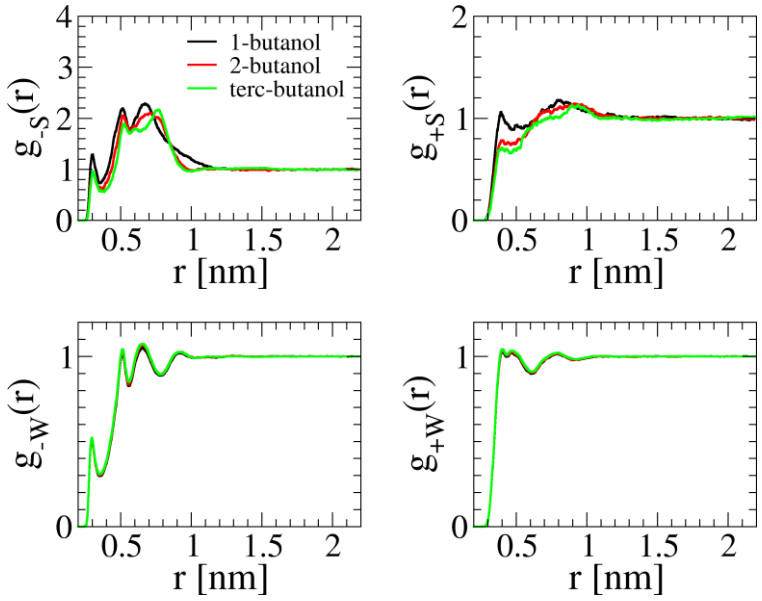

Figure S13. Radial distribution function of 0.6 M butanol (S) and water (W) around PIL-anion (-) and PIL-cation (+). It is evident that the butanol is more attracted to the PIL-anion

than to cation, and for both PIL-ions, the **order is 1-butanol > 2-butanol > terc-butanol**. In contrast, the water solution structure around PIL-ions is almost indistinguishable in all three cases.

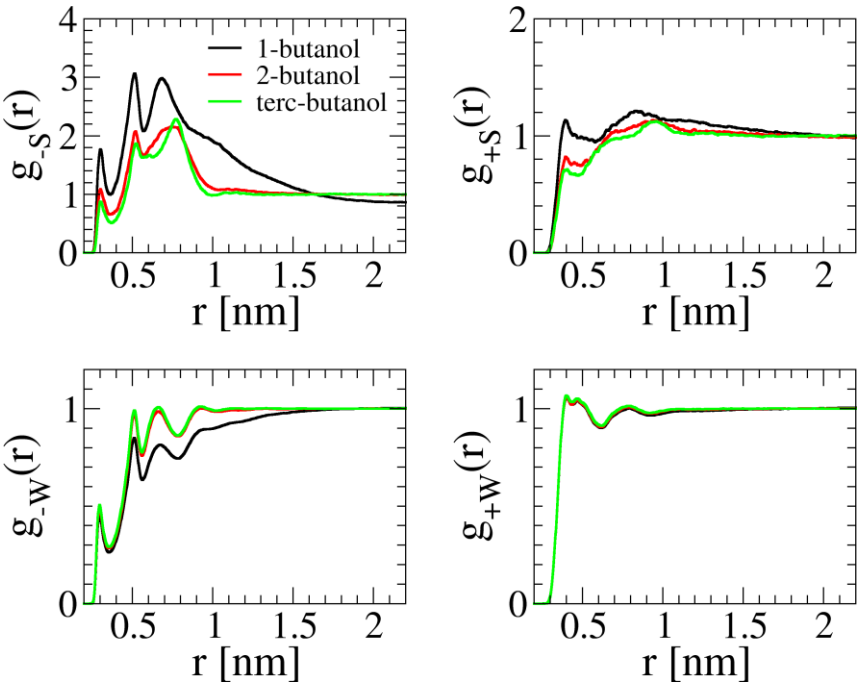

Figure S14. Radial distribution function of 1.2 M butanol (S) and water (W) around PIL-anion (-) and PIL-cation (+). It is evident that the butanol is more attracted to the PIL-anion than to cation, and for both PIL-ions, the order is **1-butanol > 2-butanol > terc-butanol**. In contrast, the water solution structure around the PIL-ions is almost indistinguishable in three cases. *Please note that the 1-butanol starts to aggregate at this concentration (it is around its experimental water solubility limit). This is also evident from water-butanol solution structure (data not shown).*

Applying eq. (S-MD1), the water and cosolvent excess adsorption numbers were obtained (see **Figure S15** and the summary in **Table S2**). Positive values can be interpreted as

adsorption, negative values as exclusion. We found specific adsorption of the cosolvent (at both concentrations) to the cation-anion pair in the order:

1-butanol >> 2-butanol > terc-butanol >> water

This order is in accord with the experimental PIL solubility and curvature data. We note that the butanol adsorption was found always to be higher to the PIL-anion as compared to the PIL-cation.

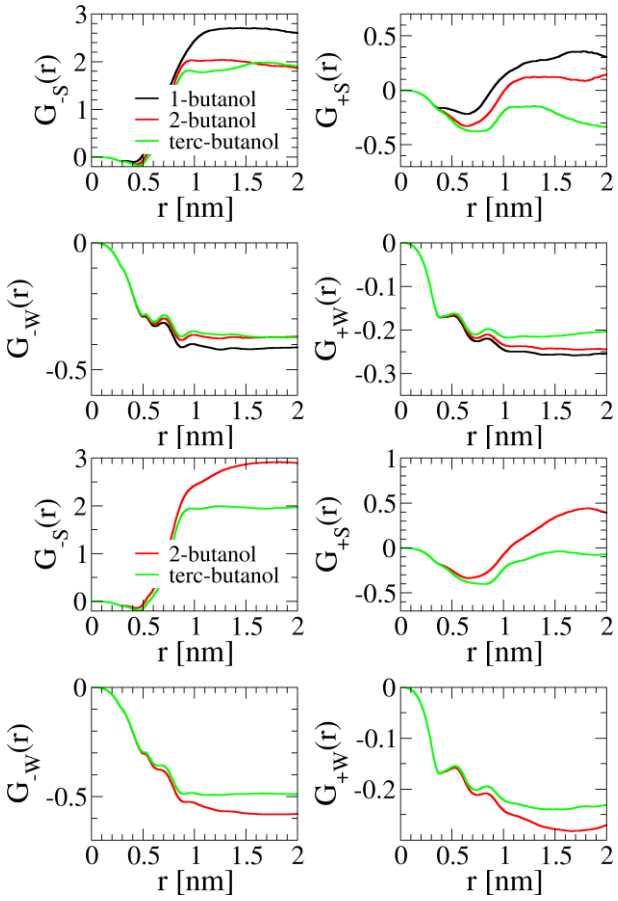

Figure S15. Running Kirkwood-Buff integrals ($\rho_j G_{ij} = N_{ij}^{ex}$, i.e. concentration normalized adsorption number) for butanol (S) and water (W) around the PIL-anion (-) and the PIL-cation (+), evaluated by eq. (S-MD1) for the lower butanol concentration (0.6 M) on the left and at the higher butanol concentration (1.2 M) on the right. The thermodynamically relevant value is read from the plateau (i.e. in the region where g(r) reaches unity); here we have chosen the value at r = 1.5 nm. The observed order is 1-butanol >> 2-butanol > terc-butanol for both PIL-

ions. In contrast, the water solution adsorption around PIL-ions is similar and negative in all butanol solutions. Please note that the 1-butanol starts to aggregate at 1.2M concentration, for clarity this data are not presented.

Table S2. Summary of the thermodynamic parameters – Kirkwood-Buff integrals G_{ij}, Adsorption numbers N_i^{ex}, and preferential binding coefficient Γ, for one PIL-ion-pair in water-butanol solutions. Two butanol concentrations are compared (0.6 M and 1.2 M), and the neat water solution serves as a reference for water adsorption (N_W^{ex}). See also **Figure S16**, for a presentation of the concentration dependence of these parameters.

System	$\rho_{butanol}$	$G_{PIL\text{-}W}$	$G_{PIL\text{-}S}$	N_W^{ex}	N_S^{ex}	Γ
neat water	0	-0.49	ND	-26.7	ND	ND
1-butanol	0.6	-0.66	3.15	-34.7	1.8	2.2
1-butanol	1.2	ND	ND	ND	ND	ND
2-butanol	0.6	-0.62	2.15	-32.6	1.2	1.6
2-butanol	1.2	-0.88	3.1	-46.2	3.5	4.5
terc-butanol	0.6	-0.59	1.75	-31.0	1.0	1.3
terc-butanol	1.2	-0.74	1.9	-38.9	2.2	3.0

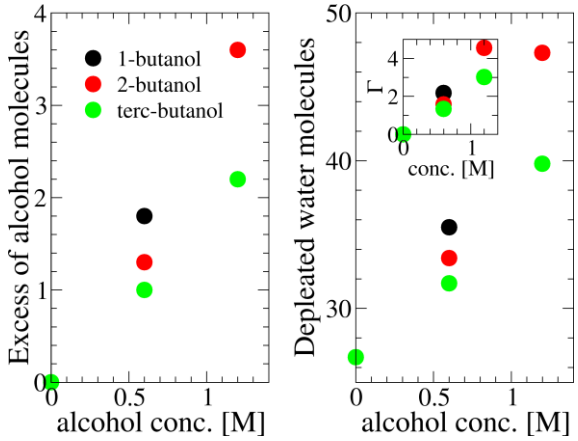

Figure S16. Excess of butanol molecules (left) and the exclusion of water molecules (right) from the PIL-ion-pair presented as a function of butanol concentration (see Table S2). The preferential binding coefficient Γ (excess of butanol over water), is provided as an inset of the right figure, and the positive value documents the enrichment of PIL-ion-pair vicinity in butanol. The observed order of the butanol excess is **1-butanol >> 2-butanol > terc-butanol**. The same order holds for the water exclusion.

3.3. Mechanistic interpretation at microscopic level:

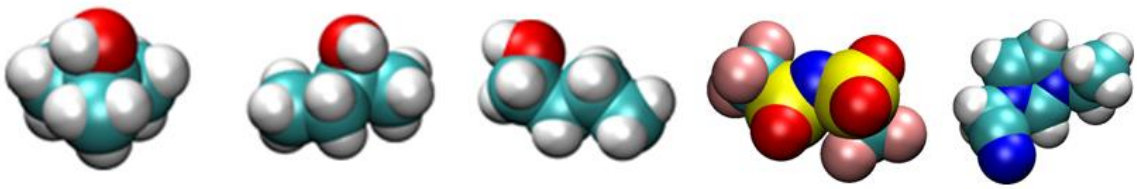

Figure S17. Space filling representation of isobutanol, 2-butanol, 1-butanol Tf_2N anion, and imidazolium based IL cation (left to right). Colors: H-white, C-cyan, O-red, S-yellow, N-blue, F-pink. All molecules are modelled as flexible in the MD simulation**.**

Already from the structure and hydration of alcohol and PIL molecules (see Figure S17), we can raise three points which are likely responsible for the butanol preferential adsorption to PIL ion-pair in aqueous solutions.

(1) Water hydrates only weakly the hydrophobic regions (fluoro- and hydrocarbon groups) of PIL ions.

(2) Butanol isomers are increasingly hydrophobic 1-butanol > 2-butanol > terc-butanol, i.e., the large hydrophobic part is weakly hydrated, since the effect of the hydroxyl group induces only local hydrophilicity.

(3) Butanol isomers have very limited H-bonding propensities (only a single OH group), and the PIL ions can serve only as H-bonding acceptors (via S=O, and C≡N group).

To sum up, water, as a highly polar medium with dynamic H-bonding networks, is preferably depleted from the PIL vicinity (first 1-2 solvation layers) and replaced by less polar butanol molecules. The effect is more pronounced for the PIL anion, as documented in **Figure S18** on the examples of the solvent/cosolvent distribution for three investigated butanol isomers. The more polar regions of IL, such as $-O_2S-N-SO_2-$, stay hydrated.

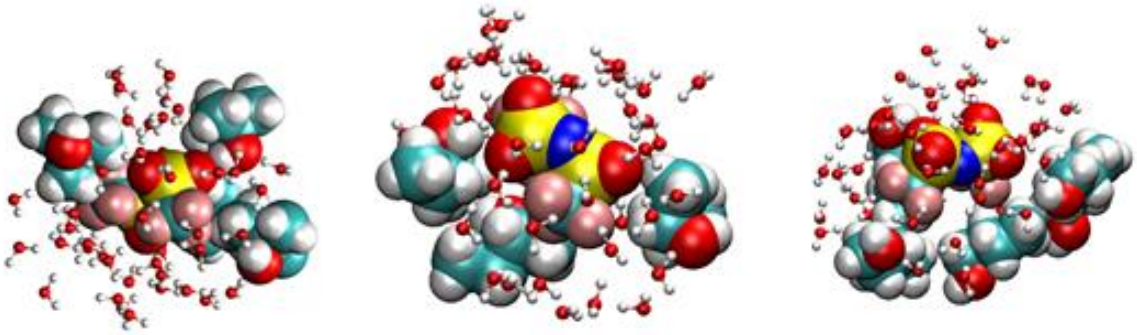

Figure S18. Illustrative distribution of butanol molecules (in space filling representation) and of water molecules (spheres-and-sticks) around the bis-triflate anion. From left to right: isobutanol, 2-butanol, and 1-butanol. Note the hydrophobic regions of bis-triflate are solvated by butanol, while polar regions bis-triflate by water.

As clearly visible from **Figure S18**, there is only minor difference between the structural arrangements of the butanol isomers in PIL vicinity. However, based on their different hydrophobicity, ordered from most hydrophobic to least hydrophobic, **1-butanol > 2-butanol > *terc*-butanol**, and the different propensity of butanol isomers to create an H-bond, **1-butanol > 2-butanol > *terc*-butanol** (best H-bond to worst), we suppose that the 1-butanol physico-chemical properties compete best with water for interactions with our PIL-ion-pair. We note that the PIL-cation-anion pair formation is observed to be of transient nature and is quantitatively the same in all three water-butanol solutions (data not shown).

3.4. Summary – action of butanol isomers on the actuator

Our MD simulations and subsequent analysis provide clear evidence that 1-butanol better solvates the PIL ion-pair compared to 2-butanol and terc-butanol by preferentially adsorbing mainly to the bis-triflate anion and replacing a large number of less preferably located water molecules. This butanol excess leads to a decrease in interfacial tension and the systems

'opens up' to more favorable butanol adsorption. From a mechanical point the osmotic pressure of the solvent increases and the polymer swells.

5. Cooperative actuation of PCMVImTf$_2$N-PAA membrane actuators.

Figure S19. A photograph showing that the "membrane coil" in Figure 4 could be suspended in air by poking a syringe needle through it, indicating that the coil is comprised of entangled and interlocked membrane stripes. Note: the membranes in Figure S16 were not painted with red color and show their original yellowish color.

References to SI

[S1] M. K. Khan, W. Y. Hamad, M. J. MacLachlan, Adv Mater 2014, 26, 2323.

[S2] W.-E. Lee, Y.-J. Jin, L.-S. Park, G. Kwak, Adv Mater 2012, 24, 5604.

[S3] K. D. Harris, C. W. M. Bastiaansen, D. J. Broer, Macromol Rapid Commun 2006, 27, 1323..

[S4] Q. Zhao, J. W. C. Dunlop, X. L. Qiu, F. H. Huang, Z. B. Zhang, J. Heyda, J. Dzubiella, M. Antonietti, J. Y. Yuan, Nat Commun 2014, 5, 4293.

[S5] D. Van der Spoel, E. Lindahl, B. Hess, G. Groenhof, A. E. Mark, H. J. C. Berendsen, J Comput Chem 2005, 26, 1701.

[S6] a) J. N. C. Lopes, A. A. H. Padua, Theor Chem Acc 2012, 131; b) X. P. Wu, Z. P. Liu, S. P. Huang, W. C. Wang, Phys Chem Chem Phys 2005, 7, 2771.

[S7] C. Caleman, P. J. van Maaren, M. Y. Hong, J. S. Hub, L. T. Costa, D. van der Spoel, J Chem Theory Comput 2012, 8, 61.

[S8] G. Bussi, D. Donadio, M. Parrinello, J Chem Phys 2007, 126.

[S9] M. Parrinello, A. Rahman, J Appl Phys 1981, 52, 7182.

[S10] H. J. C. Berendsen, J. R. Grigera, T. P. Straatsma, J Phys Chem 1987, 91, 6269.

[S11] V. Pierce, M. Kang, M. Aburi, S. Weerasinghe, P. E. Smith, Cell Biochem Biophys 2008, 50, 1.